The Astrophysical Journal Letters, 822:L7 (5pp), 2016 May 1 doi:10.3847/2041-8205/822/1/L7

FAST RADIO BURSTS FROM THE INSPIRAL OF DOUBLE NEUTRON STARS

Jie-Shuang Wang[1,2], Yuan-Pei Yang[1,2], Xue-Feng Wu[3,4], Zi-Gao Dai[1,2], and Fa-Yin Wang[1,2]
[1] School of Astronomy and Space Science, Nanjing University, Nanjing 210093, China; dzg@nju.edu.cn
[2] Key Laboratory of Modern Astronomy and Astrophysics (Nanjing University), Ministry of Education, China
[3] Purple Mountain Observatory, Chinese Academy of Sciences, Nanjing 210008, China
[4] Joint Center for Particle, Nuclear Physics and Cosmology, Nanjing University-Purple Mountain Observatory, Nanjing 210008, China
Received 2016 March 3; revised 2016 April 12; accepted 2016 April 13; published 2016 April 22

ABSTRACT

In this Letter, we propose that a fast radio burst (FRB) could originate from the magnetic interaction between double neutron stars (NSs) during their final inspiral within the framework of a unipolar inductor model. In this model, an electromotive force is induced on one NS to accelerate electrons to an ultra-relativistic speed instantaneously. We show that coherent curvature radiation from these electrons moving along magnetic field lines in the magnetosphere of the other NS is responsible for the observed FRB signal, that is, the characteristic emission frequency, luminosity, duration, and event rate of FRBs can be well understood. In addition, we discuss several implications of this model, including double-peaked FRBs and possible associations of FRBs with short-duration gamma-ray bursts and gravitational-wave events.

Key words: gamma-ray burst: general – gravitational waves – radio continuum: general – stars: neutron

1. INTRODUCTION

Fast radio bursts (FRBs) are flashes with durations of order 1 ms at typical frequencies of ∼1 GHz. Up to now, 17 FRBs have been detected (Lorimer et al. 2007; Keane et al. 2012, 2016; Thornton et al. 2013; Burke-Spolaor & Bannister 2014; Spitler et al. 2014, 2016; Champion et al. 2015; Masui et al. 2015; Petroff et al. 2015; Ravi et al. 2015). Recently, a new burst (FRB 150418) and its fading radio transient lasting ∼6 days were reported (Keane et al. 2016). The host galaxy associated with this transient has been identified to be an elliptical galaxy with redshift $z = 0.492 \pm 0.008$.

However, whether or not this radio transient is an afterglow of FRB 150418 remains controversial. On one hand, Williams & Berger (2016) and Vedantham et al. (2016) argued that the radio transient may be faring from an active galactic nucleus. On the other hand, Li & Zhang (2016) statistically examined the chance coincidence probability to produce such a transient and found that the possibility of being an afterglow of FRB 150418 is not ruled out. Despite this debate, the observed dispersion measures, which are in the range of a few hundreds to few thousands pc cm^{-3}, still provide strong evidence that at least some FRBs including FRB 150418 are at cosmological distances.

Many models have been proposed to explain the properties of FRBs, including giant flares from magnetars (Popov & Postnov 2010; Kulkarni et al. 2014), annihilations of mini-black holes (BHs; Keane et al. 2012), mergers of two neutron stars (NSs; Totani 2013), NS–BH mergers (Mingarelli et al. 2015), double white dwarf mergers (Kashiyama et al. 2013), blitzars (Falcke & Rezzolla 2014; Zhang 2014), eruptions of nearby flaring stars (Loeb et al. 2014), collisions between NSs and asteroids/comets (Geng & Huang 2015), giant pulses from pulsars (Connor et al. 2016; Cordes & Wasserman 2016), and charged BH–BH mergers (Zhang 2016a). However, as argued by Zhang (2016b), some of these models are clearly inconsistent with a high kinetic energy required by the radio transient after FRB 150418 if this afterglow is indeed true.

Although observations of FRB 110523 associated with a dense magnetized plasma (Masui et al. 2015) and the repeating FRB 121102 (Spitler et al. 2014, 2016; Scholz et al. 2016) seem to disfavor catastrophic event models including old NSs, as indicated by classification of gamma-ray bursts (GRBs), at least two distinct classes of FRBs should exist (Keane et al. 2016). This conclusion is also suggested by a recent statistical analysis (Li et al. 2016). Furthermore, the plausible radio afterglow of FRB 150418 associated with an elliptical galaxy shows that this FRB is likely to be contemporaneous with a short GRB, and thus the NS–NS merger model of FRBs is still favored (Keane et al. 2016; Zhang 2016b).

In the NS–NS merger scenario, the physical mechanism of FRBs remains a mystery. In this Letter, we study the physical processes of forming an FRB within the framework of a unipolar inductor model. This model has been proposed to describe a kind of magnetic interaction in NS–NS systems, by which energy can be extracted during the binary inspiral (Lai 2012; Piro 2012). This leads to electromagnetic radiation before the final merger. Even though Totani (2013) and Mingarelli et al. (2015) argued that the mergers of NS–NS/BH binaries could be progenitors of FRBs, they have not carried out an analysis and modeling of relevant physical processes. In addition, our work is different from Hansen & Lyutikov (2001). These authors assumed a pulsar-like coherent radio radiation during the NS–NS inspiral, whereas here we focus on the energy extraction in the unipolar inductor model. The orientation of radio radiation is quite different between our and Hansen & Lyutikov's models. This, in fact, implies different observational associations of FRBs with other counterparts like short GRBs.

This Letter is organized as follows. In Section 2, we briefly introduce the unipolar inductor model based on the NS–NS merger scenario. In Section 3, we apply it to an FRB and constrain the model parameters. In Section 4, we present our summary and discussions.

2. THE UNIPOLAR INDUCTOR MODEL

The unipolar inductor model was originally put forward in the Jupiter–Io system (Goldreich & Lynden-Bell 1969). This

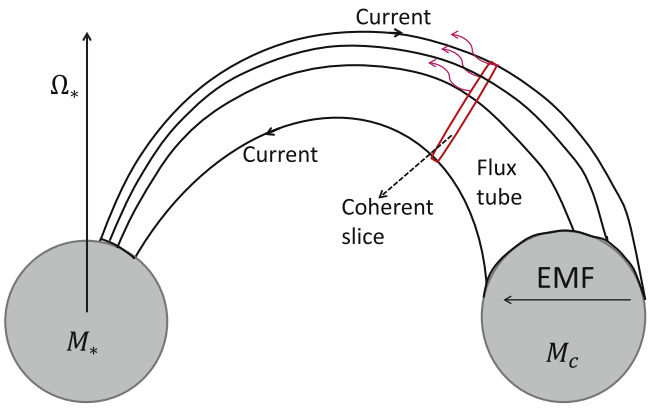

Figure 1. Schematic picture of an electric circuit based on the unipolar inductor model during the final inspiral of double neutron stars. The red block is a slice where curvature radiation of electrons is coherent.

model was then applied to several systems, such as double white dwarf binaries (Wu et al. 2002) and NS–NS/BH binaries (Hansen & Lyutikov 2001; McWilliams & Levin 2011; Lai 2012; Piro 2012). Usually, one of two NSs in this model has a much stronger magnetic field than that of the other NS. Recent simulations show that this model is still likely to be established, even if the ratio of the magnetic field strengths of two NSs is ~100 (Palenzuela et al. 2013).

Considering a primary NS with mass M_*, spin Ω_*, magnetic dipole moment $\mu_* = B_* R_*^3$, and radius R_* and its companion NS with mass M_c and radius R_c, the distance between the two NSs is a and the orbital angular velocity is Ω. We assume that $\mathbf{\Omega}_*$, $\boldsymbol{\mu}_*$, and $\mathbf{\Omega}$ are aligned for simplicity. As the companion crosses the magnetic field lines of the primary NS, an electromotive force (EMF) is generated as shown in Figure 1, $\mathcal{E} \simeq 2R_c|\boldsymbol{E}|$, where $\boldsymbol{E} = \boldsymbol{v} \times \boldsymbol{B}/c$, $\boldsymbol{B} = \boldsymbol{\mu}_*/a^3$, and $\boldsymbol{v} = (\Omega - \Omega_*) \times \boldsymbol{a}$ (Lai 2012; Piro 2012). During the inspiraling stage, spin–orbit synchronization cannot be achieved by magnetic and tidal torques (Bildsten & Cutler 1992; Kochanek 1992; Lai 1994, 2012; Ho & Lai 1999), so the spinning angular velocity of the primary NS could be much smaller than the orbital angular velocity and we assume that $|\boldsymbol{v}| \sim \Omega a$. Thus, the EMF is given by

$$\mathcal{E} \simeq \frac{2\mu R_c}{ca^2}\Omega. \tag{1}$$

The magnetic field lines exhibit like electric wires, and thus a DC circuit is established. The resistance of the circuit ($\mathcal{R}_{\rm tot}$) is generally believed to be dominated by the magnetosphere, which is in units of the impedance of free space, namely, $\mathcal{R}_{\rm tot} \simeq 2\mathcal{R}_{\rm mag} = 8\pi/c$ (Lai 2012; Piro 2012). As we show below, this magnitude of resistance is reasonable. The factor two is introduced because the circuit could be established on both sides of the binary orbit. However, the circuit is unstable since a toroidal magnetic field is produced and grows even to be comparable to the poloidal field. Thus, Lai (2012) proposed a quasi-cyclic circuit model, in which when the toroidal magnetic field is strong enough, the circuit breaks down and then the magnetic energy is released due to the reconnection process. Subsequently, the toroidal magnetic field becomes weak and the whole cycle repeats. In this case, the energy dissipation rate is (Lai 2012)

$$\dot{E}_{\rm diss} = 1.7 \times 10^{42} B_{*,12}^2 a_{30}^{-7}\ {\rm erg\ s^{-1}}, \tag{2}$$

where $B_{*,12} = B_*/10^{12}$ G and $a_{30} = a/30$ km. This is consistent with the energy dissipation rate given by the simulation of Palenzuela et al. (2013). Thus, we believe that the resistance used here is reasonable.

Even if a small fraction of the binary orbital energy is extracted by the magnetic interaction, evolution of the NS–NS binary is dominated by gravitational-wave radiation (Lai 2012), following

$$\dot{a} = -\frac{64G^3M_*^3q(1+q)}{5c^5a^3}, \tag{3}$$

where $q = M_c/M_*$ is the mass ratio of the two stars (Landau & Lifshitz 1975). For simplicity, we set $M_* = 1.4M_\odot$, $R_* = R_c = 10$ km, and $q = 1$. Thus, we obtain

$$\begin{aligned} a &= a_0\left[1 - \frac{256G^3M_*^3q(1+q)}{5a_0^4c^5}t\right]^{1/4} \\ &= 20(1 - 1695t)^{1/4}\ {\rm km}, \end{aligned} \tag{4}$$

where we set the zero time when the surfaces of the two NSs just touch with each other, i.e., $a = 20$ km at $t = 0$. Combining with Equation (2), we find the energy dissipation rate grows drastically in the last few milliseconds, which is consistent with the typical duration of an FRB.

3. MODELING AN FRB

As described by Goldreich & Julian (1969), the magnetosphere of a pulsar is filled with electrons/positrons. However, due to the EMF near the surface of the companion in our model, more electrons/positrons might be produced. We assume that the electron density n_e caused by the EMF is analogous to the space-charge density in the magnetosphere of a pulsar, and thus find

$$n_e \simeq \frac{\mathbf{\Omega}\cdot\boldsymbol{B}}{2\pi ec} \simeq 1.5 \times 10^{12} B_{*,12} a_{30}^{-9/2}\ {\rm cm^{-3}}, \tag{5}$$

where we have taken the orbital angular velocity to be $\Omega = [GM_*(1+q)/a^3]^{1/2}$.

The EMF will accelerate these electrons/positrons, while radiation cools them down. On the surface of the companion, the drift velocity of the electrons is $v_d \sim cE_\parallel/B$, where $E_\parallel$ is the parallel component of the electric field along the magnetic field, which has a small value for the magnetic field configuration in our model. Thus, the drift velocity $v_d \lesssim c$ and the curvature radius of the electron motion could be approximately the synchrotron gyration radius. The electron energy after acceleration could be determined by the balance between the "synchrotron-like" cooling and electric field acceleration, that is,

$$P_{\rm syn} \simeq \frac{1}{6\pi}\sigma_{\rm T} c\gamma^2 B^2 \sim eEc, \tag{6}$$

where $\sigma_{\rm T} = 6.65 \times 10^{-25}$ cm^2 is the Thomson scattering cross-section. Therefore, the maximum Lorentz factor, at which the electrons are accelerated by the EMF, is approximately given by

$$\gamma_{\rm max} \sim \left(\frac{6\pi e\Omega a}{c\sigma_{\rm T}B}\right)^{1/2} \simeq 370 B_{*,12}^{-1/2} a_{30}^{5/4}. \tag{7}$$

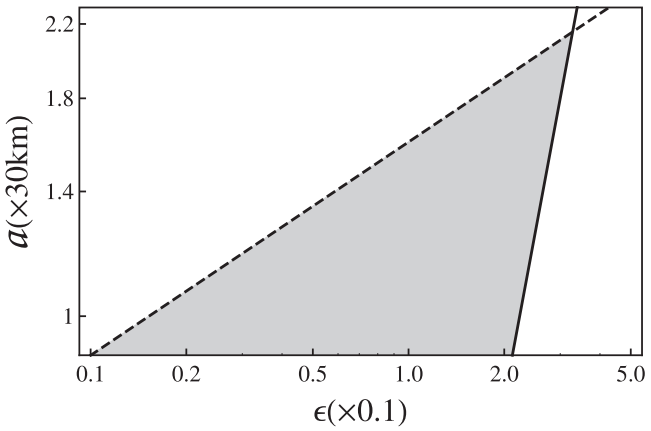

Figure 2. Constraints on the parameters a and ϵ with assumptions of $B_{*,12}=1$, $\rho_{30}=1$, and $P_{c,40}=1$. The typical frequency of observed FRBs ($\nu_{\rm curv,9}=1.4$) is taken here. Due to inequality (11), the Y-axis starts from $a\simeq 28$ km. The solid line comes from inequality (17), while the dashed line comes from inequality (18).

The acceleration time is $t_{\rm acc}\simeq \gamma_{\rm max}m_ec/eE=1.5\times10^{-15}B_{*,12}^{-3/2}a_{30}^{19/4}$ s. This is far smaller than the orbit period, which is generally of the order of ~1 ms.

The characteristic frequency of curvature radiation is

$$\nu_{\rm curv}=\frac{3c\gamma^3}{4\pi\rho}=2.4\times10^3\gamma^3\rho_{30}^{-1}\,{\rm Hz}, \tag{8}$$

where $\rho=30\rho_{30}$ km is the curvature radius and γ is the Lorentz factor of an emitting electron. For a typical FRB, we have

$$\gamma=75\rho_{30}^{1/3}\nu_{\rm curv,9}^{1/3}, \tag{9}$$

where $\nu_{\rm curv,9}=\nu_{\rm curv}/10^9$ Hz. We then discuss whether or not a photon can propagate through the plasma in the magnetosphere by considering three effects. First, the plasma frequency in the emission region is

$$\nu_p=\frac{1}{2\pi}\left(\frac{4\pi n_ee^2}{m_e}\right)^{1/2}. \tag{10}$$

In a highly magnetized magnetosphere, the plasma effect is negligible if $\nu_p<\gamma^{1/2}\nu_{\rm curv}$ (Lyubarskii & Petrova 1998), which is further written as

$$a_{30}>1.0B_{*,12}^{2/9}\gamma_2^{-2/9}\nu_{\rm curv,9}^{-4/9}, \tag{11}$$

where $\gamma_2=\gamma/10^2$ and we have taken the electron density of the emission region to be roughly that of the acceleration region. Second, the cyclotron absorption in the magnetosphere is generally considered in pulsar physics, whose optical depth is given by Lyubarskii & Petrova (1998):

$$\tau_{\rm cyc}\simeq 2\times10^{-3}B_{*,12}^{3/5}P_*^{-9/5}\nu_{\rm curv,9}^{-3/5}\gamma_2^{-3/5}, \tag{12}$$

where $P_*=2\pi/\Omega_*$ and the electron number density outside of the flux tube (see Figure 1) has been assumed to be described by the Goldreich–Julian density. Thus, the cyclotron absorption can be ignored if $P_*>0.03B_{*,12}^{1/3}\nu_{\rm curv,9}^{-1/3}\gamma_2^{-1/3}$ s. Third, the characteristic distance (l) of a photon due to the Thomson scattering is (Lyubarskii & Petrova 1998)

$$l=\frac{1}{(1-\beta_e\cos\theta)\bar{n}_e\sigma_{\rm T}}=\frac{1.5\times10^{14}\,{\rm cm}}{\bar{n}_{e,10}(1-\beta_e\cos\theta)}, \tag{13}$$

where β_ec is the velocity of an electron, θ is the angle between the motion directions of the electron and photon, and $\bar{n}_{e,10}=\bar{n}_e/10^{10}\,{\rm cm}^{-3}$ has been assumed to be the mean electron number density of the magnetosphere. The light cylinder R_L for a pulsar with period P_* is $R_L=cP_*/2\pi=4.88\times10^9(P_*/1\,{\rm s})\,{\rm cm}\ll l$. Therefore, we conclude that a photon with frequency of order 1 GHz can propagate freely through the magnetosphere.

For a single relativistic electron or positron, the emission power of curvature radiation is $P_e=2\gamma^4e^2c/3\rho^2$. The electron cooling timescale due to curvature radiation is

$$t_{\rm cool}=\frac{\gamma m_ec^2}{P_e}=1.6\times10^9\rho_{30}^2\gamma_2^{-3}\,{\rm s}. \tag{14}$$

An electron will spend a typical time $t_{\rm circuit}\sim a/c=0.1$ ms in moving from the companion to the primary star. Thus, the electron will not be cooled down by curvature radiation. This indicates that once an electric circuit is established (or broke up), electrons will fill (or leave) the flux tube (see Figure 1) immediately. Therefore, it is reasonable to assume that the total volume of the emitting region is approximately given by $V_{\rm tot}\simeq 2V_{\rm FT}\sim\pi^2R_c^2a/3$, where the factor of two is due to the fact that the flux tube is established on both sides of the binary orbit, and the volume of the flux tube (approximated by a circular cone with height $\pi a/2$) is taken to be $V_{\rm FT}\sim\pi^2R_c^2a/6$.

However, once the wavelength of radiation is comparable to the size of the emission region, the emission is coherent (Ruderman & Sutherland 1975). In this case, the volume of a coherent slice (see Figure 1) is roughly $V_{\rm coh}\sim\pi R_c^2\times c/\nu_{\rm curv}$. Thus, the number of slices is $N_{\rm slices}=V_{\rm tot}/V_{\rm coh}\simeq\gamma^3a/4\rho$, which is similar to the estimate of Falcke & Rezzolla (2014). The total electron number in the emission region is roughly $N_{\rm tot}\simeq n_eV_{\rm tot}$, where n_e is the electron number density of the emission region and is assumed to be equal to that of the acceleration region. Meanwhile, what should be noted is that for coherent radiation, the Lorentz factors of emitting electrons should be in a certain range. Therefore, the electrons participating in coherent radiation might be smaller, that is, $N_e\simeq\epsilon N_{\rm tot}$ with $\epsilon=0.1\epsilon_{0.1}\lesssim 1$. Following Falcke & Rezzolla (2014), the total power of coherent radiation is

$$P_c\simeq N_{\rm slices}^{-1}N_e^2P_e\simeq4.6\times10^{39}\gamma\epsilon_{0.1}^2B_{*,12}^2\rho_{30}^{-1}a_{30}^{-8}\,{\rm erg\,s^{-1}}, \tag{15}$$

and together with Equation (9), we obtain

$$P_c\simeq3.5\times10^{41}\epsilon_{0.1}^2B_{*,12}^2\rho_{30}^{-2/3}a_{30}^{-8}\nu_{\rm curv,9}^{1/3}\,{\rm erg\,s^{-1}}. \tag{16}$$

We now constrain the model parameters. The total power of coherent radiation should be smaller than the energy dissipation rate due to the unipolar inductor, $P_c\lesssim\dot{E}_{\rm diss}$, which is also written by

$$a_{30}\gtrsim0.2\epsilon_{0.1}^2\rho_{30}^{-2/3}\nu_{\rm curv,9}^{1/3}. \tag{17}$$

A typical FRB generally has a luminosity $P_c \gtrsim 10^{40}$ erg s^{-1}, which leads to

$$a_{30} \lesssim 1.6\epsilon_{0.1}^{1/4} B_{*,12}^{1/4} \rho_{30}^{-1/12} P_{c,40}^{-1/8} \nu_{\rm curv,9}^{1/24}, \quad (18)$$

where $P_{c,40} = P_c/10^{40}$ erg s^{-1}. An example of constraints on a and ϵ for a successful FRB from inequalities (11), (17), and (18) is shown in Figure 2. The right-side region of the solid line is unphysical because $P_c > \dot{E}_{\rm diss}$, while the left-side region of the dashed line means that FRBs may be too faint to be detected. When the separation a becomes smaller than ∼28 km, the curvature emission might be absorbed and further turn into X-ray and/or γ-ray emission when the electrons hit the surface of the primary star (McWilliams & Levin 2011). Thus, we find that the coherent radio emission is observable in the range of $a \sim 60$ km to ∼28 km for a typical primary pulsar with $B_* = 10^{12}$ G and an appropriate fraction ϵ.

The current event rate of FRBs is roughly $\sim 2.8 \times 10^3$ Gpc^{-3} yr^{-1} at redshift $z \lesssim 1$ with normalization of the daily all-sky FRB rate of the order of $\sim 10^4$ (Zhang 2016b), while the "realistic estimate" rate of NS–NS mergers is $\sim 10^3$ Gpc^{-3} yr^{-1} and the "plausible optimistic estimate" rate is $\sim 10^4$ Gpc^{-3} yr^{-1} (Abadie et al. 2010). Thus, the FRB rate is well consistent with the NS–NS merger rate.

4. SUMMARY AND DISCUSSIONS

In this Letter, we have studied the physical processes of an FRB and explained its main features within the framework of the unipolar inductor model of inspiraling NS–NS binaries. The companion non-magnetic NS crosses the magnetosphere of the primary highly magnetized NS and simultaneously produces an EMF, by which electrons are accelerated to an ultra-relativistic speed instantaneously. These electrons then move along magnetic field lines and generate coherent curvature radiation as shown in Figure 1. The total power and timescale of coherent radiation are well in agreement with a typical FRB.

Our model is clearly different from the short GRB/FRB association scenario proposed by Zhang (2016a), who suggested that the inspiral of a charged BH–BH binary forms an electric circuit and produces an induced magnetic field. This field, if corotating with the BHs around the center of mass of the binary system, would behave like a "giant pulsar." The coherent curvature radiation from the magnetosphere of this pulsar-like object could explain the properties of FRBs.

Inequalities (11), (17), and (18) have given constraints on the model parameters. For a larger orbital separation or a lower magnetic field, the flux of an FRB might be too low to be observed. For a higher magnetic field, we might observe an FRB in a different orbit period. This indicates a double-peaked FRB if the emission during two orbit periods is observed. In addition, there are some connections among FRBs, short GRBs/afterglows, and gravitational-wave events in our model. In what follows, we would like to discuss several implications of this model in some detail.

First, since the direction of curvature radiation might not be aligned with the orbital angular momentum that is just the direction of a subsequent short GRB, it is not necessary to observe an FRB and a short GRB contemporaneously. However, it seems easier to detect an FRB associated with a short GRB afterglow since an afterglow generally has a wider opening angle than a GRB itself does (Keane et al. 2016).

Second, the coherent curvature radiation could not point to us at all of the times during one orbital period. Thus, for binaries with stronger magnetic interaction, we might observe an FRB signal during two or more periods, which might be responsible for an FRB with double peaks (Champion et al. 2015).

Third, X-ray emission is predicted in the unipolar inductor model (Hansen & Lyutikov 2001; McWilliams & Levin 2011; Lai 2012; Palenzuela et al. 2013). Following McWilliams & Levin (2011), a fraction of energy will be kept in the form of plasma kinetic energy. When this plasma reaches the primary NS, a hot spot might be induced. However, this hot spot would be observed only for a source at distance $\lesssim$100 Mpc (McWilliams & Levin 2011).

Fourth, the merger of double NSs after an FRB would leave behind a rapidly rotating BH (Paczýnski 1986; Eichler et al. 1989) or a millisecond pulsar/magnetar (Dai et al. 2006; Zhang 2013). Such objects have been widely argued as both the central engine of short GRBs and one of the gravitational-wave events that could be detected by the advanced LIGO. What should be noted is that these two kinds of central objects have different properties of gravitational waves, which, if detected, could further identify post-merger compact stars. Therefore, it would be expected to see possible associations of FRBs with short GRB afterglows and gravitational-wave events in the future. The detections/non-detections of such associations would confirm/constrain/exclude our model.

Finally, Spitler et al. (2016) and Scholz et al. (2016) recently reported their detections of 10 and 6 additional bright bursts from the direction of FRB 121102, respectively. This repeating FRB is obviously distinct from the other non-repeating FRBs and thus challenges all the catastrophic event models. Very recently, we proposed a novel DC circuit model, in which a repeating FRB could originate from a highly magnetized pulsar encountering with an asteroid belt of another star (Dai et al. 2016). During each pulsar–asteroid impact, an electric field induced on the elongated asteroid near the pulsar's surface can drive an electric circuit. We showed that this model can well account for all the properties of FRB 121102, including the emission frequency, luminosity, duration, and repetitive rate. We also predicted the occurrence rate of similar repeating sources.

We thank an anonymous referee for useful comments and constructive suggestions that have allowed us to improve our manuscript significantly. We also thank Yong-Feng Huang, Xiang-Yu Wang, and Bing Zhang for useful discussions. This work was supported by the National Basic Research Program ("973" Program) of China (grant No. 2014CB845800) and the National Natural Science Foundation of China (grant Nos. 11573014, 11322328, 11433009, 11422325, and 11373022).

REFERENCES

Abadie, J., Abbott, B. P., Abbott, R., et al. 2010, CQGra, 27, 173001
Bildsten, L., & Cutler, C. 1992, ApJ, 400, 175
Burke-Spolaor, S., & Bannister, K. W. 2014, ApJ, 792, 19
Champion, D. J., Petroff, E., Kramer, M., et al. 2015, MNRAS, submitted (arXiv:1511.07746)
Connor, L., Sievers, J., & Pen, U.-L. 2016, MNRAS, 458, L19
Cordes, J. M., & Wasserman, I. 2016, MNRAS, 457, 232
Dai, Z. G., Wang, J. S., Wu, X. F., & Huang, Y. F. 2016, arXiv:1603.08207
Dai, Z. G., Wang, X. Y., Wu, X. F., & Zhang, B. 2006, Sci, 311, 1127

Eichler, D., Livio, M., Piran, T., & Schramm, D. N. 1989, Natur, 340, 126
Falcke, H., & Rezzolla, L. 2014, A&A, 562, A137
Geng, J. J., & Huang, Y. F. 2015, ApJ, 809, 24
Goldreich, P., & Julian, W. H. 1969, ApJ, 157, 869
Goldreich, P., & Lynden-Bell, D. 1969, ApJ, 156, 59
Hansen, B. M. S., & Lyutikov, M. 2001, MNRAS, 322, 695
Ho, W. C. G., & Lai, D. 1999, MNRAS, 308, 153
Kashiyama, K., Ioka, K., & Mészáros, P. 2013, ApJL, 776, L39
Keane, E. F., Johnston, S., Bhandari, S., et al. 2016, Natur, 530, 453
Keane, E. F., Stappers, B. W., Kramer, M., & Lyne, A. G. 2012, MNRAS, 425, L71
Kochanek, C. S. 1992, ApJ, 398, 234
Kulkarni, S. R., Ofek, E. O., Neill, J. D., Zheng, Z., & Juric, M. 2014, ApJ, 797, 70
Lai, D. 1994, MNRAS, 270, 611
Lai, D. 2012, ApJL, 757, L3
Landau, L. D., & Lifshitz, E. M. 1975, The Classical Theory of Fields (Oxford: Pergamon)
Li, L., Huang, Y., Zhang, Z., Li, D., & Li, B. 2016, arXiv:1602.06099
Li, Y., & Zhang, B. 2016, arXiv:1603.04825
Loeb, A., Shvartzvald, Y., & Maoz, D. 2014, MNRAS, 439, L46
Lorimer, D. R., Bailes, M., McLaughlin, M. A., Narkevic, D. J., & Crawford, F. 2007, Sci, 318, 777
Lyubarskii, Y. E., & Petrova, S. A. 1998, A&A, 337, 433
Masui, K., Lin, H.-H., Sievers, J., et al. 2015, Natur, 528, 523
McWilliams, S. T., & Levin, J. 2011, ApJ, 742, 90
Mingarelli, C. M. F., Levin, J., & Lazio, T. J. W. 2015, ApJL, 814, L20
Paczýnski, B. 1986, ApJL, 308, L43
Palenzuela, C., Lehner, L., Liebling, S. L., et al. 2013, PhRvD, 88, 043011
Petroff, E., Bailes, M., Barr, E. D., et al. 2015, MNRAS, 447, 246
Piro, A. L. 2012, ApJ, 755, 80
Popov, S. B., & Postnov, K. A. 2010, arXiv:0710.2006
Ravi, V., Shannon, R. M., & Jameson, A. 2015, ApJL, 799, L5
Ruderman, M. A., & Sutherland, P. G. 1975, ApJ, 196, 51
Scholz, P., Spitler, L. G., Hessels, J. W. T., et al. 2016, ApJ, submitted (arXiv:1603.08880)
Spitler, L. G., Cordes, J. M., Hessels, J. W. T., et al. 2014, ApJ, 790, 101
Spitler, L. G., Scholz, P., Hessels, J. W. T., et al. 2016, Natur, 531, 202
Thornton, D., Stappers, B., Bailes, M., et al. 2013, Sci, 341, 53
Totani, T. 2013, PASJ, 65, L12
Vedantham, H. K., Ravi, V., Mooley, K., et al. 2016, ApJL, submitted (arXiv:1603.04421)
Williams, P. K. G., & Berger, E. 2016, ApJL, in press (arXiv:1602.08434)
Wu, K., Cropper, M., Ramsay, G., & Sekiguchi, K. 2002, MNRAS, 331, 221
Zhang, B. 2013, ApJL, 763, L22
Zhang, B. 2014, ApJL, 780, L21
Zhang, B. 2016a, arXiv:1602.04542
Zhang, B. 2016b, ApJ, in press (arXiv:1602.08086)